Outdoor Measurements of Spherical Acoustic Shock Decay

by

Sarah M. Young

A senior thesis submitted to the faculty of

Brigham Young University-Idaho

In partial fulfillment of the requirements for the degree of

Bachelor of Science

Department of Physics

Brigham Young University – Idaho

December 2015

BRIGHAM YOUNG UNIVERSITY – IDAHO

DEPARTMENT APPROVAL

of a senior thesis submitted by

Sarah Young

This thesis has been reviewed by the research committee, senior thesis coordinator, and department chair and has found to be satisfactory.

_____	_____
Date	Todd Lines, Advisor
_____	_____
Date	Ryan Nielson, Committee Member
_____	_____
Date	Evan Hansen, Senior Thesis Coordinator
_____	_____
Date	Steve Turcotte, Interim Department Chair

ABSTRACT

Outdoor Measurements of Spherical Acoustic Shock Decay

Sarah Young

Department of Physics

Bachelor of Science

Prior anechoic measurements of a small acetylene-oxygen balloon explosion were used to study spherical weak-shock decay over short ranges [2]. In this Thesis, longer-range measurements conducted at the Bonneville Salt Flats with a larger balloon are described. Waveform and spectral characteristics and comparisons of the peak pressure decay with an analytical weak-shock model are presented. Weak shocks persist to at least 305 m, with an amplitude decay that is predicted reasonably well using this model. Deviations are discussed in the context of atmospheric effects and nonlinear ground reflections. This research describes that presented in Young *et al*. [1]

Acknowledgements

This research was funded through the National Science Foundation REU program and the analysis was conducted under a Brigham Young University Mentoring Environment grant. Many thanks to Dr. Kent Gee, Dr. Tracianne Neilsen, and Kevin Leete for their many hours of research tutelage. Also, the assistance of many members of the Brigham Young University Acoustics Research Group was invaluable during the Salt Flats measurements.

Thank you to the BYU-Idaho Physics Department faculty for fostering an environment of joyous learning and growth.

Lastly, to my parents whose love, patience, and encouragement have carried me further than I ever imagined.

Table of Contents

List of Figures

Chapter 1

Introduction

1.1 Background and Previous Research

The current research as presented in this thesis and the recent article by Young[1], is a continuation of work conducted by Muhlestein[2] *et al*. on spherical acoustic shock propagation over a distance. Shocks follow nonlinear acoustic theory, where wave amplitude and velocity are interdependent, meaning that as amplitude increases, so does the wave velocity.[3] Linear sound waves are those encountered in everyday speech and noise, which travel at 343 m/s (called c_0), and follow a sinusoidal shape when plotted as pressure at a point over time. Because of the increased velocity of a nonlinear acoustic wave, or shock, the compressions travel faster than the rarefactions, as shown in Figure 1 for a wave traveling to the left. Eventually, this creates a situation where the compressions are stacked on top of the rarefactions (Figure 1, red line with dots). It is not physically possible for the wave amplitude to have three values at one time, so in reality, a near-discontiuity of pressure is created at what would normally be the zero pressure point between crests and valleys, shown in red with dots in the lower portion of Figure 1. A characteristic sawtooth shock wave is formed, filled with higher frequency harmonics and traveling faster than c_0, 343 m/s.

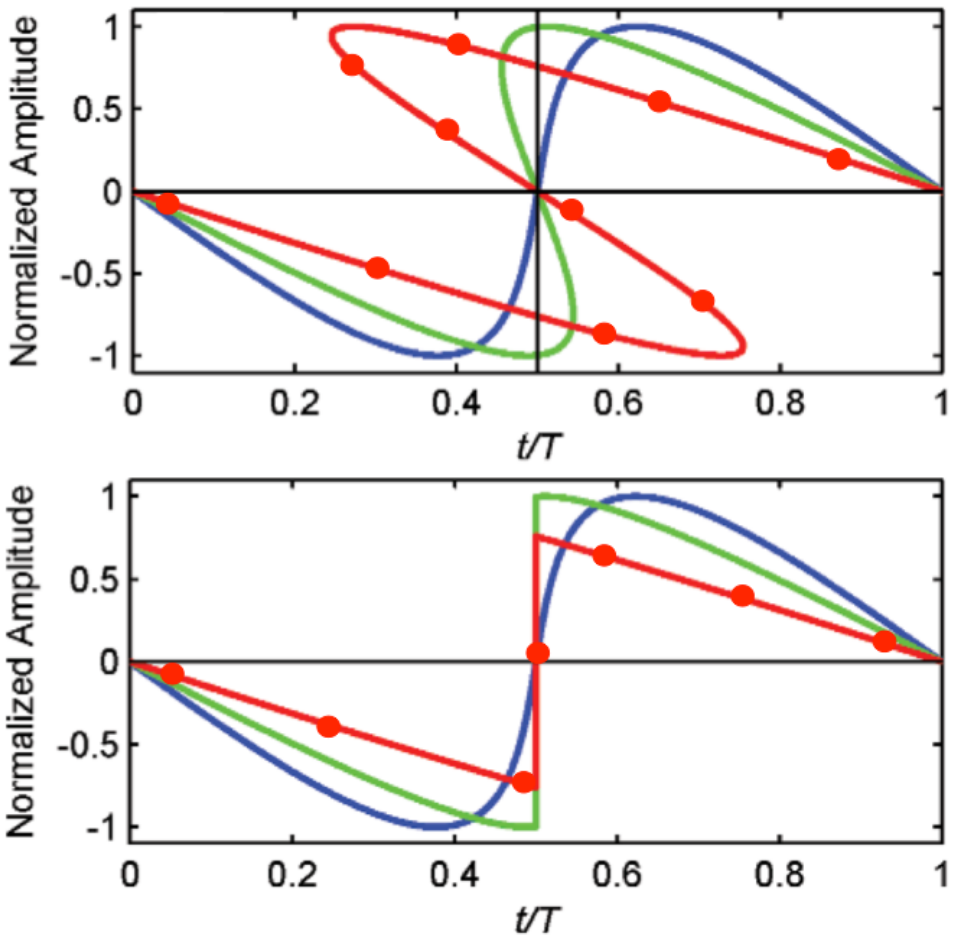

Figure 1 - In a wave traveling to the left, compressions (positive amplitude) are traveling faster than the rarefactions (negative amplitude), leading to the eventual physical overlap of rarefactions and compressions (top figure, red with dots), an impossible situation in reality. Instead a near-discontinuity, or shock, is created at the reflection point, as seen in the lower figure (red with dots). The blue and green waves show the progression of the sinusoidal wave into a shock. The horizontal axis is time divided by the period of the previously sinusoidal wave.[3]

Muhlestein's work used small balloons filled with either hydrogen or oxygen/acetylene as the shock source, ignited in an anechoic chamber with microphones arranged 1 to 4 meters from the blast. The shock wave pressure decay over a distance was compared to that modeled by weak-shock theory, as developed by Blackstock.[4] This theory uses the Earnshaw solution to the Burgers differential equation and ultimately predicts spherical acoustic pressure decay over a distance from a small point source shock. This mathematical result is shown below in Equation 1.

$$p_{shock} = \frac{r_0 p_0}{r} \frac{\sqrt{1 + 2\eta \ln(r/r_0)} - 1}{\eta \ln(r/r_0)}, \quad (1)$$

where $\eta = \frac{p_0}{t_0} \frac{\beta r_0}{\rho_0 c_0^3}$.

These equations use the peak pressure at a known distance from the source (r_0), along with other parameters describing the non-linearity of air, to predict the pressure at any radial distance (r) from the source. This equation will be discussed in more detail in section 3.4.

While Muhlestein's research was largely pedagogical in purpose, he also validated weak-shock's predictions in his analysis of pressure decay from balloon explosions. Figure 2 illustrates his findings, showing his anechoic data in black dots compared to the theory in red. The pressure is transformed into Sound Pressure Level (L_{pk} in dB with respect to a reference pressure of 20 μPa, also called SPL) using the equation $L_{pk} = 20 \log_{10}(P/20\times 10^{-6})$. The gray line in Figure 2 shows how the SPL would decay if it were low-amplitude

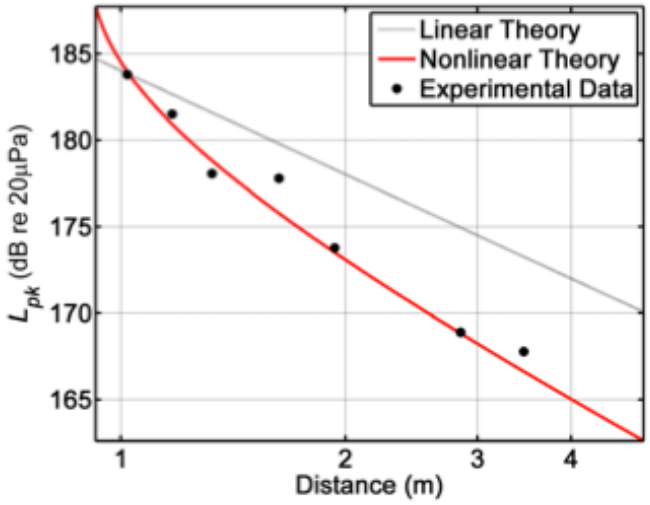

Figure 2 - Results of analysis of weak-shock theory as presented by Muhlestein *et al.*[2]

sound. In the low-amplitude case, the SPL decreases linearly on a log scale.

The research shown in this thesis uses many of Muhlestein's methods but on a much larger scale. Balloons were filled with up to 70 times more oxygen and acetylene and were exploded in an outdoor setting. This allowed for pressure testing much further than is possible in an anechoic chamber, but also created the potential for interference from factors like weather and reflections off of structures. Experimental results from this large-scale testing could then be compared to weak-shock theory and an analysis conducted of whether shocks can still be considered only "weak" at such high amplitudes.

Acoustic shocks can be classified by size and propagation in a variety of ways, and previous studies have delved into the subject. Primarily since WWII and the advent of the atomic bomb, extensive research has been conducted characterizing the range and scale of explosions. Monographs on explosions in air by Kinney and Graham[5] as well as Baker[6] have provided an empirical look at chemical and nuclear explosions. This led to explosion scaling laws as defined by an ANSI Standard,[7] which has since been used by Ford[8] to study the acoustic blast over a variety of surfaces from plastic explosives. Other acoustic shock theories have been examined in the context of underwater explosions,[9] N-wave spark shocks,[10] more plastic explosions,[11] and Gatling gun muzzle blasts.[12] Related research has been conducted on cylindrical ballistic shocks,[13,14] the acoustics of supersonic projectiles. Vernon,[15] at BYU, has investigated the acoustic properties of different gases inside exploding balloons.

While these studies provide valuable insight, the research presented here evaluates weak-shock theory using data from a nearly point source, allowed to propagate outdoors for distances not previously studied. The care taken in measurement location and time of day

resulted in clean data. Because of this, meaningful and detailed analysis can be carried out. The analysis is conducted using pressure waveforms, one-third octave Sound Exposure Level (SEL), and the spherical propagation curve of weak-shock theory.

Chapter 2

Methods

2.1 Overview of Experimental Design

Balloons needed to be bigger to test acoustic shock distance propagation on a large scale, and create a shock wave detectable out a mile from the initial blast. Balloons were filled with combustible gases, mounted on a tripod, and ignited. The ensuing explosion generated heat and flames, but also an acoustic shock wave that spread spherically from the blast site. The pressure readings from this shock wave were captured on microphones distributed at distances from 1 to 1600 m from the blast. To minimize interference from acoustic wave reflections, and lacking an anechoic chamber on this scale, the experiment required a large open space, flat, and free from structures or mountains, however, using an outdoor setting allowed for potential interference from wind or other atmospheric pressure fronts. In addition, the shock wave's unavoidable reflection off of the ground would also interfere with acoustic pressure readings of the shock wave.

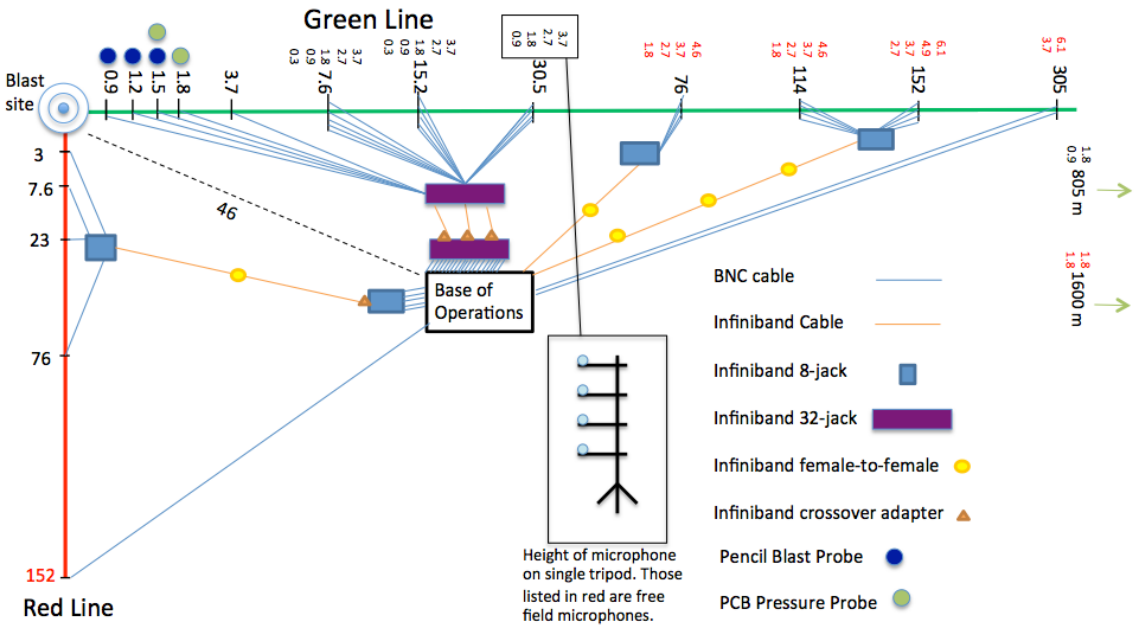

Figure 3 - Experimental layout at the Bonneville Salt Flats. All microphone connections required a microdot cable to connect the microphone to the BNC cable. The distances marked on the green or red line indicate the position of a tripod at that location (in meters). The small numbers listed next to the distances are the height of the microphones on each tripod (in feet). Any tripod with no small numbers listed had one microphone at a height of 3.7 m (such as those listed on the red line). The tripods at 805 m and 1600 m were on the green line. The tripods at 15.2 and 30.5 m were moved to 27.4 and 35 m, respectively, mid-testing. Figure is not to scale.

2.2 Setup

The experiment was conducted on Utah's Bonneville Salt Flats on 15 July 2014 from 6:00 to 10:00 am MDT, with set up and system checks completed the previous evening. The Salt Flats provided an acoustically hard, flat, and homogeneous surface coupled with a large open region, free from reflecting structures. A central point for the balloon explosions was determined along the Bonneville Speedway. Two lines of tripods led away from the explosion center, one along the Speedway, called the "green line" with 14 tripods, and one perpendicular to the Speedway, called the "red line" with 5 tripods. Tripods ranged in maximum height from 3.7 to 6.1 meters (12 to 20 feet) high, and held as many as 5

Figure 4 - (Left) Picture of microphone array on the flats with balloon mounting cradle on far right. (Right) View of cables and tripods from base camp position.

microphones or blast probes. The full layout, including cables and connectors used, microphone positions, and microphone heights, is shown in Figure 3.

For the microphones positioned within 4 m of the balloon, the tripods were offset from the green line to reduce wave scattering among the many tripods, as shown in Figure 4. Mid-testing the tripods at 15.2 and 30.5 meters from the source were moved to 27.4 and 35 meters, respectively, in order to better capture ground reflection phenomena potentially occurring in that distance from the source.

2.3 Equipment Specifications

All microphones used were manufactured by G.R.A.S., each with a 6.35 mm (1/4 inch) diameter of varieties 46BG, 40BD, and 40BE. The 46BG and 40BD microphone types have especially low sensitivities, designed for near-field rocket noise measurements.[16] Also, the microphones closer to the source were all “pressure” microphones and had significantly lower sensitivities than those further from the source, known as “free field” microphones.

The lower the sensitivity of the microphone, the higher the pressure it can sense without clipping. Clipping is when the microphone technologically is overwhelmed, leading to inaccurate pressure readings. All microphones were mounted on thin, round dowels attached to the tripod and were oriented with their diaphragm either sky-ward, toward the blast, or perpendicular to the blast depending on microphone type (a pictorial representation of this is shown in Figure 5). The microphones had their protective grid caps removed an hour before testing. While the grid cap protects the fragile diaphragm from foreign bodies like dust, it can also generate inaccurate pressure readings as the sound waves interact with the slotted metal. All microphones underwent a thorough sensitivity calibration process using G.R.A.S. calibration software in the weeks prior to the test, involving an examination of the microphone preamplifier for signal stability over time and the microphone for its range of frequency response. Only PCB piezoresistive pressure gages, specifically designed for blast noise measurements, were used in the region under 3.0 m (10 ft) from

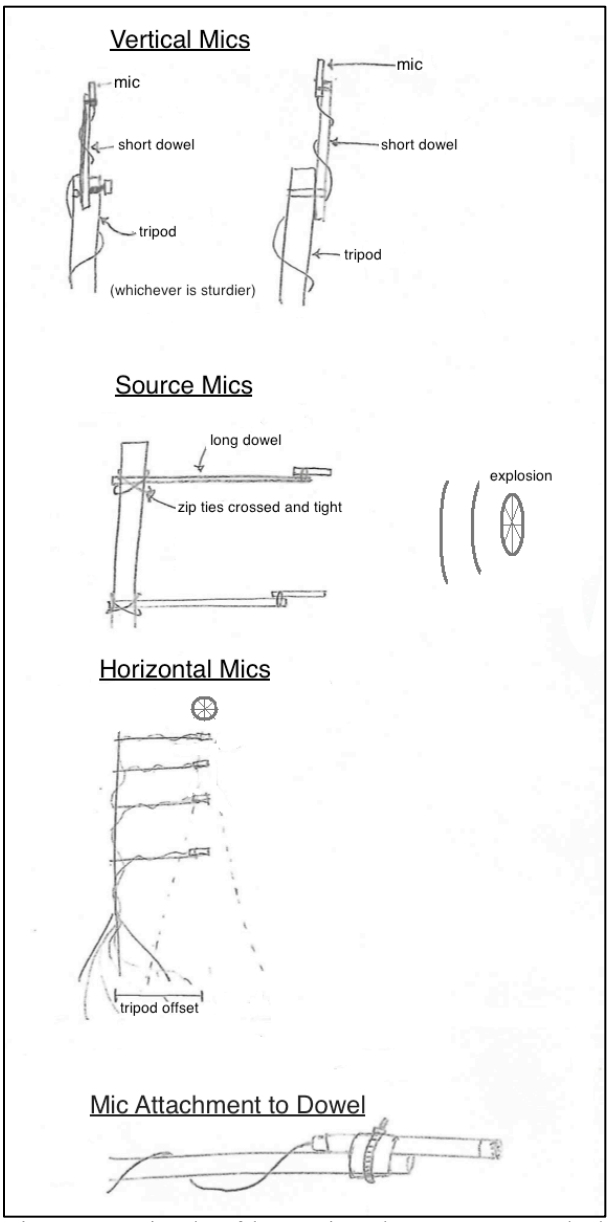

Figure 5 – Visuals of how microphones were attached to the dowels and tripods in relation to the position of the blast site. Free field mics are pointed with their diaphragm toward the source and pressure mics have their diaphragm perpendicular to the source.

the blast.

2.4 Balloon Ignition and Testing

Spherical latex balloons (to better approximate a point source) were filled with a stoichiometric combination of 0.143mol oxygen to 0.057mol acetylene chosen to maximize the acoustic shock.[2] Balloon sizes of diameter 84, 69, 56, 43, 36, and 20 cm (33, 27, 22, 17, 14, and 8 inches) were prepared and ignited in order to study a range of shock sizes. To ensure the balloons were filled to the proper ratios, we prepared circumference rings to fit to the balloon as it was filled with first acetylene to a specified circumference, then oxygen to the final circumference. Those filling the balloons used both ear and eye protection at all times during the filling process (Figure 6). The filled balloon was carried to the blast sight and mounted on a 3.7 m (12 ft) high tripod with a conical wire cradle to keep the balloon in place. A model rocket igniter was strapped to the base of the balloon, with the two leads connected via alligator clips to a BNC cable, which stretched the distance to the base of operations. A button trigger was used to deliver the voltage necessary to ignite the balloon. The size of the explosion depended largely on balloon size, although for the largest balloons the explosion radius was visually estimated at around 3 m (Figure 7). The ensuing acoustic shock wave traveled spherically from the source, generating readings of pressure over time (Pascal vs seconds) on all microphones and other pressure gauges. All researchers present wore double hearing protection and a countdown was used to both ensure hearing safety and begin data collection.[17]

Data were recorded using National Instruments PXI-4462 dynamic signal acquisition

Figure 6 - Those filling the balloons with oxygen and acetylene used plastic rings to gauge the diameter of the filled balloon and determine if it had the right amount of gas. Those filling the balloon also wore both ear and eye protection at all times in case of accidental ignition.

devices, with the exception of the 805m data, which were recorded with a USB-9233 sampling at 50kHz. The PXI-4462 data were recorded at the maximum sampling rate, 204.8kHz. The electric signals were converted to binary using a LABVIEW-based acoustics software developed by BYU over years of research.

2.5 Potential Errors

Atmospheric conditions were studied for the entire duration of testing, since any atmospheric pressure changes could significantly influence the shock pressure readings. For

Figure 7 - A 33 inch diameter balloon before and after ignition.

this reason, testing began early in the morning when wind was likely to be lower on the Salt Flats. Wind speed varied between 0 and 7 m/s, depending on the test, blowing nearly perpendicular to the green line. During the measurement window, the temperature increased from 23 to 31° C with an attendant decrease in relative humidity from 28% to 19%. The ambient pressure was 87 kPa. A two-point temperature measurement during the second half of testing indicated a slight inversion with an approximate gradient of 0.2° C/m at a height of 1m above the ground. This circumstance was helpful as the data was examined for abnormalities, as will be shown.

Other potential sources of error could have occurred in the balloon filling process, as the balloons were filled with an inexact number of moles of gas. In addition, the vans driven to the salt flats could have generated a small acoustic reflection, but compared to the size of the original blast, any interference would have been undetectable.

2.6 Data Analysis

Matlab script was used during post-experiment analysis to convert the binary files into pressure vs time shock waveforms viewed as Matlab figures (see Appendix A). A single waveform, such as that shown in the top left of Figure 8 shows the pressure readings from one microphone for the duration of one balloon blast. To make the pressure readings usable for comparison over distance, each waveform was examined by hand and the initial peak pressure was extracted and listed in a spreadsheet along with the test ID, balloon size, time of test, tripod location, and height of microphone. To find the exact peak pressure required working around Gibbs-phenomena,[2] an error in the analog to digital conversion that overestimates the peak pressure. When clear artifacts were found, they were accounted for by examining the slope immediately following the initial shock. In addition, some microphones

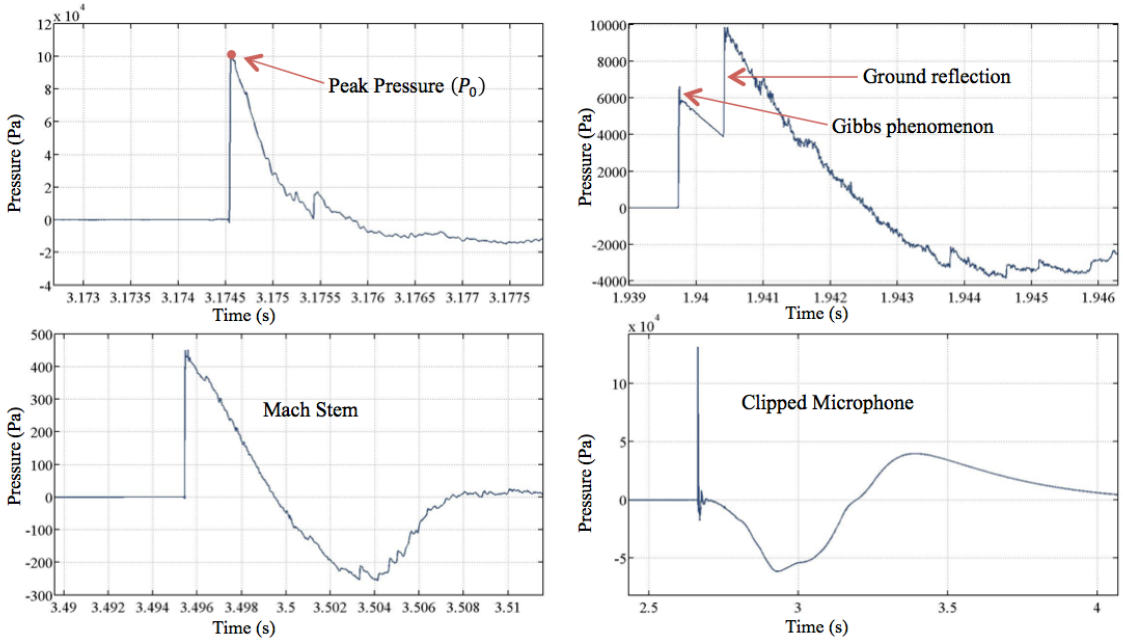

Figure 8 - Pressure vs time waveform of a normal peak pressure (Top Left). Waveform showing Gibbs ringing, an overestimation of the pressure due to data acquisition errors, and also the ground reflection approaching the incident wave (Top Right). Waveform where the incident and reflected waves have combined to form a Mach stem (Bottom Left). Microphone where the pressure was so high, microphone sensitivity was overwhelmed resulting in a "clipped" reading. Zoomed into the spike at 2.6 seconds, the readings look like a regular waveform, but the significant drop and rise in pressure readings for a few seconds after the spike indicate a malfunction (Bottom Right).

closer to the source experienced clipping. This is where pressure readings are underestimated when the actual pressure was higher than could be sensed by the microphone sensory equipment. Clipping was easy to see in the waveform, but meant the readings were useless. Fortunately, clipping occurred rarely and only on the largest balloons. Lastly, when the portion of the spherical shock moving downward hits the ground, it reflects back upwards. Through an eventual decrease in path length difference as the reflected wave speeds up, the reflected wave catches the original wave, which is propagating horizontal to the ground. Since the ground reflections were expected, the high pressures were just recorded as found. However, the reflections off of the rough ground of the salt flats generated more inexact undulations of peak pressure, thus more possibility of error.

Chapter 3

Analysis and Results

3.1 Overview

Three main analysis methods were used for studying the data. The geometry of the shock waveforms were examined, especially how they changed over distance from the blast. This included an analysis of wave reflections, the impact of atmosphere, and also shock rise time. These methods will be discussed below using figures showing pressure waveforms versus time at a variety of distances. Similar conclusions are found using a plot of one-third octave band sound exposure level (SEL). Lastly, waveform peak pressures shown as a function of distance are compared to theoretical models of weak-shock propagation. The accuracy of both the data and theoretical models are discussed. While the bulk of the results presented are those found for one 56 cm diameter balloon explosion, the analysis of many others show similar conclusions.

3.2 Shock Waveform Analysis

Each shock waveform consists of the pressure reading on a given microphone over time, as shown in Figure 9 at a succession of distances ranging from 0.9 to 805 m. Each of the waveforms shown comes from the same balloon explosion, all at a height of 3.7 m (12 ft). The overpressure, the measurement value above atmospheric pressure, is shown in a 10 ms window with vertical lines every 2 ms, and the dashed red line indicating the initial peak

overpressure. For example, on the top left waveform in Figure 9, the distance from the source is 0.9 m with a peak shock (p_{sh}) of 152 kPa, equivalent to a L_{pk} of 198 dB re 20 μPa, an Sound Pressure Level (SPL) value rounded to the nearest decibel.

Examining the waveforms in Figure 9, the shock itself broadens significantly, especially between 0.9 and 76 m as the shock travels supersonically, faster than the ambient sound speed of 348 m/s (ambient speed adjusted for current temperature). After 76 m, the shock is traveling within 1 m/s of ambient sound speed so maintains roughly the same width for a few hundred meters but still with the abrupt rise typical of a shock. Starting at the 7.6 m waveform, another shock wave is visible within the 10 ms window. This is the ground reflection, caused by the spherical shock wave reflecting off of the hard salt surface and

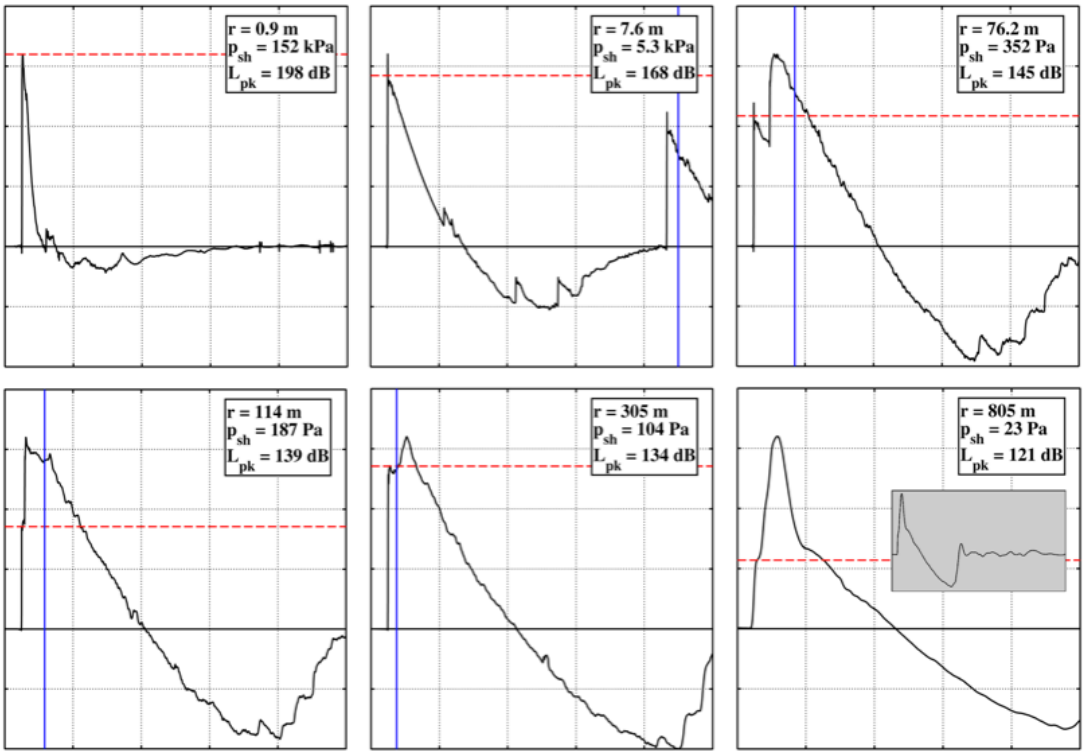

Figure 9 - Shock waveforms for a 56 cm diameter balloon explosion at distances of 0.9, 7.6, 76.2, 114, 305, and 805 meters from the source. The horizontal time axis is marked with grid lines indicating 2 ms. The dashed red line shows the peak pressure of the incident wave, while the blue line indicates where geometry and time gap delay analysis predict the location of the ground reflection. The bottom right waveform features an insert of the full waveform at 805 m.

eventually catching up with the incident wave as distance from the source increases. The blue vertical line indicates where the ground reflection should be using a time gap delay (TGD) analysis. This prediction is based on path length difference, a rigid ground impedance, and a consistent wave speed. The ground reflection is about 0.5 ms early in every waveform. At a distance of 7.6 m, the time gap predicts an incoming reflection 8.4 ms after the incident wave, but the reflection arrives after just 8 ms. This pattern continues as the reflection approaches the incident wave at 76.2 m and 114 m. At 305 m, the incident wave is indistinguishable from the ground reflection, even though the time gap shows they should be distinct, even at this far distance from the source. The inaccuracies of the time gap is likely due to an assumption of a single consistent wave velocity between the incident and reflected waves, but irrespective of this, the reflection should never quite catch the incident wave with the current set of assumptions. One plausible explanation is that the path length difference between the two waves decreases with distance, because the incident wave warms the air for the reflected wave, essentially increasing the reflected wave speed by way of temperature. Literature calls this phenomenon a Mach stem,[18] where the sum pressure of the incident and reflected waves is actually slightly greater than what direct superposition would predict. However, for the purposes of peak pressure analysis, the pressure essentially doubled. Further analysis of this phenomenon was beyond the scope of this particular project.

A close analysis of the shock waveform, though not shown clearly in Figure 9, reveals a rise time of 10 μs for all the distances shown, consistent with the limits of 6.35 mm microphones.[19] This means that the pressure level measured in the microphone jumped from zero to peak pressure in essentially 3 data points, with the sampling rate limit of 204.8 kHz. This shock rise time is maintained until 305 and 805 meters. These two distances correspond

to a rise time of points/sampling rate = 3pts/(204800pt/s) = 15 μs and 7pts/(50000pt/s) = 140 μs, respectively, allowing us to see the shock attenuation as the distance increases.[11] In other words, the increase in time for the shock to rise to its peak value indicates that the shock has been significantly slowed and warped by distance and atmospheric absorption. This is often called shock thickening.

The appearance of an extra peak on the 114 m waveform at around 1.2 sec is confusing considering the ground reflection has almost merged with the incident wave at this point. A larger extra peak is visible on the 305 and 805 m waveforms as well, suggesting the peak is an acoustic reflection off of something further than the ground, but still close enough and large enough to have a consistent presence in the data. Since there were no large structures present, the reflections must have occurred through atmospheric interaction. Weather measurements taken at the time of testing revealed an increase in temperature with height during the experiment, similar to a circumstance described by D. Keith Wilson in his paper discussing sound refraction, in the near-ground atmosphere.[20] The shock waves projecting upward off of the spherical source refracted through the temperature-dependent atmosphere and eventually bent downward, increasing pressure further down the line of microphones, just as described by Wilson. In addition to evidence of this in the waveforms, the insert in the 805 m waveform shows the same wave for an extended time period. The U-like structure of the negative pressure portion is characteristic of atmospheric interference similar to those studied in sonic booms,[21] giving further evidence of atmospheric refraction in the current experiment.

Other slight deviations in the waveforms, such as those visible between 4 and 6 ms on the 7.6 m waveform are likely pressure deviations due to the non-uniform nature of the

exploding balloons. Though the balloons were a close approximation to a point source, the explosions were not instantaneous, nor did all of the gases burn in a perfect sphere.

3.3 Sound Exposure Level

A close examination of Figure 10 reiterates many of the conclusions reached from Figure 9. Figure 10 shows the Sound Exposure Level (SEL) versus frequency, as found using a one-third octave band FFT analysis. Using one-third octave band means the FFT frequency bins were centered and integrated around three segments of the regular octave bands (1 octave per doubling of frequency with 1000 Hz at the center). For example, this means that if a normal octave frequency were 63 Hz with 125 Hz as the next octave, the third-octave frequencies would include 80 and 100 Hz as well. In Figure 10, SEL vs frequency in Hz is shown for microphones multiple distances from the source, examining the same 56 cm

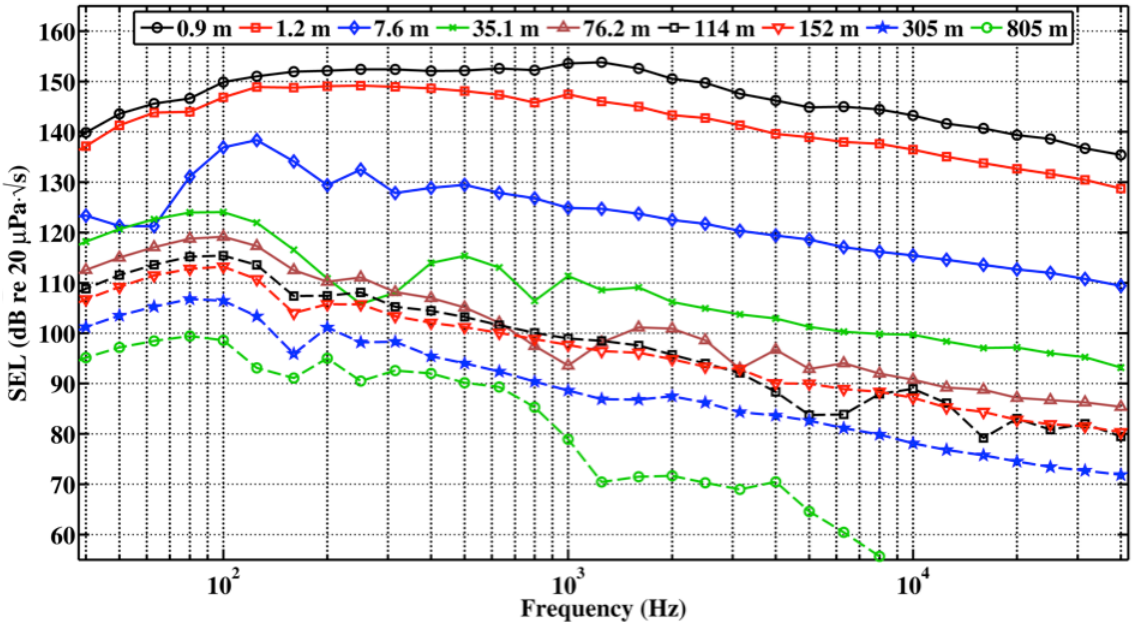

Figure 10 - Spectral Analysis vs. Sound Exposure Level (SEL) at various distances for a 56 cm diameter balloon explosion.

diameter balloon explosion as shown in Figure 9. There is a peak frequency of roughly 1000 Hz in the closest two distances, 0.9 and 1.2 m from the source, but this quickly decays to lower frequencies, corresponding to the physical shock spreading as described earlier. The decibel levels decrease by about six dB with each doubling of distance, and the lowered characteristic frequency of about 100 Hz and a consistent slope is maintained thereafter indicating that the shock wave is maintaining the same frequency content, even with the ground reflection. The $10\ \mu s$ rise time corresponds to the general negative 10 dB/decade slope as shown for every distance until 305 m, where the slope approaches 12 dB/decade with the stronger shock wave attenuation.[1] At 805 m, the high frequency content rolls off much earlier, at about 700 Hz, due to both the low amplitude non-shock propagation of the wave and atmospheric interference. The gradual merging of the ground reflection with the incident wave is not visible at 0.9 and 1.2 m since the ground reflection did not arrive with sufficient amplitude or speed to be included in the third-octave integration. Beginning with the 7.6 m and continuing through the 114 m spectra, interference minima and maxima appear at increasingly higher frequencies as the path length difference between the incident and reflected waves decreases. This interference pattern stops suddenly at 152 m when the two waves have fully merged, creating one continuous wavefront.

3.4 Peak Pressure Propagation

With the corresponding conclusions from both waveform and SEL analysis, a comparison between data and theory becomes much more meaningful. The shock wave has behaved as expected out to at least 305 m with any other trends explainable by known atmospheric conditions at the time. This allows us to trust peak pressure measurements and

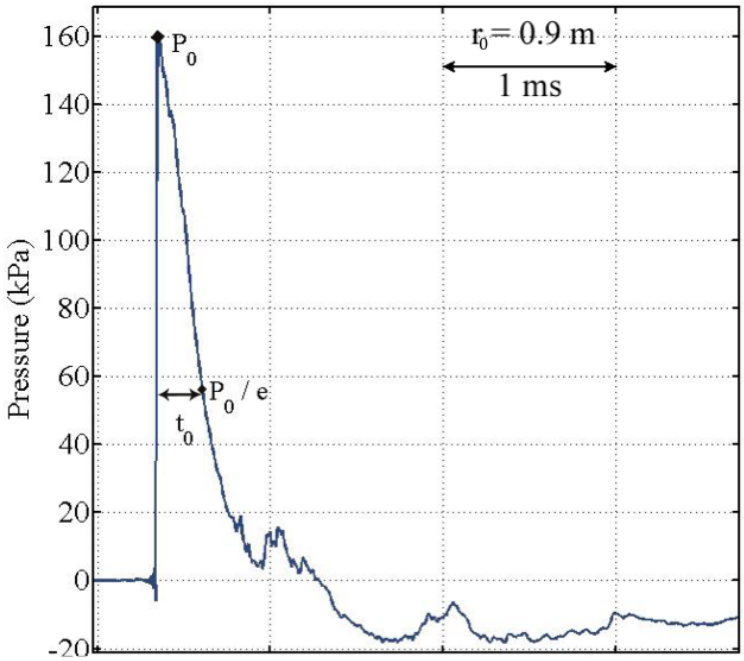

Figure 11 - A waveform showing P_0, r_0, and t_0.

thus compare weak shock theory to our data trend. With each initial peak shock value for each shock wave, we apply Muhlestein's[2] equations (equation 1 in Chapter 1) for spherical shock decay over a distance and compare it with our data.

To more fully understand the equation, p_{shock} is the pressure level of the shock wave as a function of distance from the shock source, r. To fill the initial conditions of the predictive weak-shock decay curve, a point is pulled from the data, one initial peak pressure and its corresponding distance from the source, and that specific waveform is analyzed. The parameters of r_0, p_0, and the bundle of constants in η are filled as follows from this waveform: P_0 the peak pressure, r_0 the distance from the source of the shock wave, β the coefficient of nonlinearity (1.201 in air), ρ_0 the density of air (1.21 kg/m^3), and c_0 the ambient speed of sound (348 m/s in salt flats conditions). The variable t_0 is called initial decay time, the time for the peak pressure to decay to e^{-1} of its original value. As an example using the waveform shown in Figure 11, P_0 is 160 x10^3 Pa, r_0 is 0.9 m, and t_0 is 0.2 ms. The values,

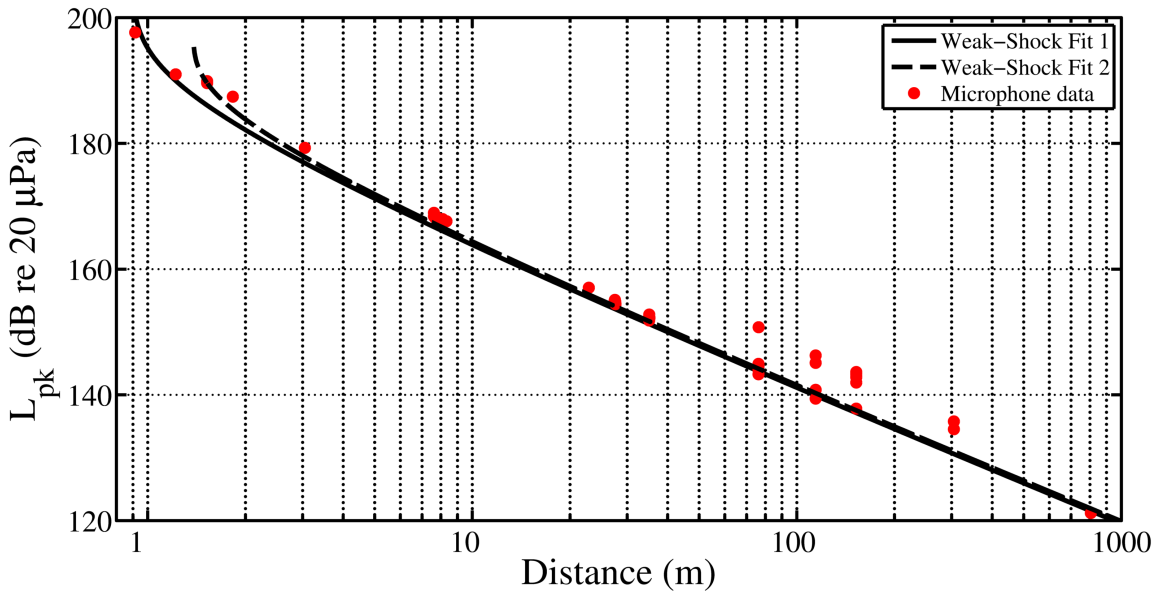

Figure 12 - Weak-shock propagation trend from a 56 cm diameter balloon. The red dots are the experimental data, the solid line, a weak-shock fit using initial conditions from $r_0 = 0.9$m, and the dashed line a weak-shock fit using initial conditions from $r_0 = 1.5m$.

when placed in equation 1, generate a curve of pressure versus distance. The values of P_0, r_0, and t_0 could be pulled from any waveform, but a more accurate graph is produced with a microphone closer to the source and more reliable in its data, thus typifying initial conditions more accurately.

Changing pressure into Sound Pressure Level (L_{pk} in dB), and plotting L_{pk} over distance, r, gives the graph shown as fit 1 in Figure 12. The red points are the actual data taken, while the solid curve is where weak-shock theory predicts the data will occur. The dashed line labeled fit 2 indicates the theoretical curve using initial conditions pulled from the data point at 1.2 m. There was some question as to whether the pressure gauge at 0.9 m was inside the explosion, so to further verify conclusions both fits were examined closely. While the fits diverge slightly in the near-field, they coalesce after 4 m from the source, maintaining the same slope and supporting the same conclusions.

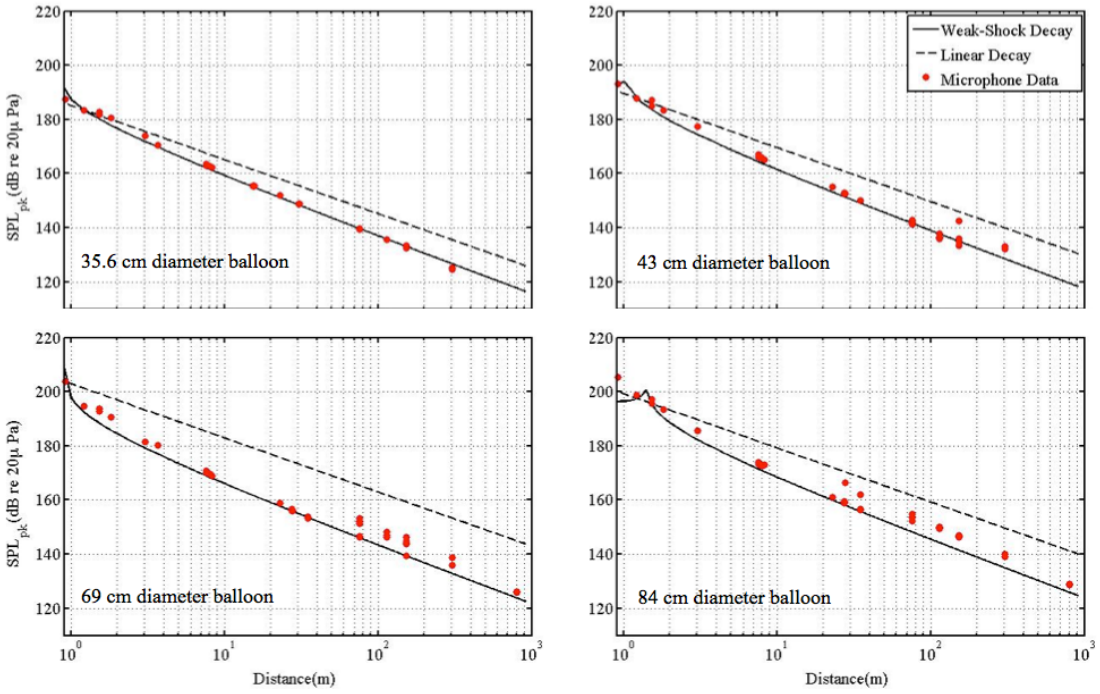

Figure 13 - The SPL vs distance curves for four different balloon sizes. 35.6 cm diameter (top left), 43 cm diameter (top right), 69 cm diameter (bottom left), and 84 cm diameter (bottom right). The 35.6 cm balloon.

Figure 12 shows the L_{pk} data closely aligning within ± 5 dB to spherical shock decay as predicted by weak-shock theory. The exception to this is the 6 dB rise after the wave become a Mach stem, visible in Figure 12 at just under 80 m, but the decay slope still follows the same trend. Given this result, it appears that weak-shock theory is an accurate predictor of nonlinear acoustic decay for even outdoor shocks approaching 200 dB. This result is similar to that found by Bass, *et al.*[13] and Wright,[10] both of whom include very similar graphs showing exponentially decaying peak pressure using the ANSI[7] model for comparison, although for a much lower SPL and smaller range. Ford, *et al.*[8] also used the ANSI model, but with limited correspondence of data to theory.

What is shown in the above weak-shock analysis is only a portion of the data available. The rest of the data set from other balloon explosions has proven to be equally reliable, as shown in Figure 13. This figure shows the same propagation curve for four other

balloon diameters. The red dots mark the data with the solid black line illustrating the weak-shock decay curve. The dashed black line shows the acoustic decay trend if the noise source followed linear propagation. While not every weak-shock trend is a perfect fit to the data, it is much closer than what linear decay would predict. We did find that the acoustic shocks with the largest amplitudes, such as the one shown in the bottom right of Figure 13, did not fit the weak-shock curve as well, however this might be expected considering the work by Pestorius and Williams[22] regarding the upper limit of weak-shock theory and the high-pressure variations that can occur. Measurements this clean out to 300 m in an outdoor setting will allow us to explore other areas of acoustics using the same data set and potentially expand weak-shock theory to the near 200 dB range.

Chapter 4

Conclusion

4.1 Conclusion

Weak-shock theory is a viable predictive tool for acoustic shock propagation over longer distances and higher decibel levels than previously studied. The outdoor testing and analysis of exploding gaseous balloons has demonstrated weak-shock theory's reliability. Using analysis tools as shown, 200 dB gaseous balloons exploded in an outdoor setting are predictable. Examining pressure waveforms in conjunction with one-third octave SEL illustrates any wave irregularities, most notably the appearance of Mach stems and atmospheric interference. Since great care was taken to eliminate other extraneous reflections, the data from the set is clean and uncluttered by unexplainable acoustic anomalies. In light of such accurate data, using it for comparison with theory was permissible. This ultimately found that the acoustic decay curves of weak-shock theory are an accurate predictor for weak shocks.

4.2 Future Work

Future work will examine the strength and appearance of Mach stems. This could encourage research into where Mach stems they occur with any given shock size and how to track them both acoustically and visually. Atmospheric phenomena pose another area of study, particularly since the impact of weather on acoustic shocks specifically has been little studied or tested.

References

[1] S. M. Young, K. L. Gee, T. B. Neilsen, K. M. Leete, "Outdoor measurements of spherical acoustic shock decay," J. Acoust. Soc. Am. **138**, EL305-EL310 (2015).

[2] M. B. Muhlestein, K. L. Gee, and J. H. Macedone, "Educational demonstration of a spherically propagating acoustic shock," J. Acoust. Soc. Am. **131**, 2422–2430 (2012).

[3] A. A. Atchley, "Not your ordinary sound experience: a nonlinear-acoustics primer," Acoustics Today **1**, 19-24 (2005).

[4] D. T. Blackstock, "Propagation of a weak shock followed by a tail of arbitrary waveform," in Proceedings of the 11th International Congress on Acoustics, Paris, France (1983), Vol. 1, pp. 305–308.

[5] G. F. Kinney and K. J. Graham, Explosive Shocks in Air (Springer, Berlin, 1985), pp. 50–136.

[6] W. E. Baker, Explosions in Air (University of Texas Press, Austin, TX, 1973), pp. 1–77, 118–163.

[7] ANSI S2.20-1983: American National Standard for Estimating Airblast Characteristics for Single Point Explosions in Air (Acoustical Society of America, Melville, NY, 2006).

[8] R. D. Ford, D. J. Saunders, and G. Kerry, "The acoustic pressure waveform from small unconfined charges of plastic explosive," J. Acoust. Soc. Am. **94**, 408–417 (1993).

[9] P. Rogers, "Weak-shock solution for underwater explosive shock waves," J. Acoust. Soc. Am. **62**, 1412–1419 (1977).

[10] W. M. Wright, "Propagation in air of N waves produced by sparks," J. Acoust. Soc. Am. **73**, 1948–1955 (1983).

[11] A. Loubeau, V. W. Sparrow, L. L. Pater, and W. M. Wright, "High frequency measurements of blast wave propagation," J. Acoust. Soc. Am. **120**, EL29–EL35 (2006).

[12] M. D. Shaw and K. L. Gee, "Acoustical analysis of an indoor test facility for a 30-mm Gatling gun," Noise Control Eng. J. **58**, 611–620 (2010).

[13] H. E. Bass, B. A. Layton, L. N. Bolen, and R. Raspet, "Propagation of medium strength shock waves through the atmosphere," J. Acoust. Soc. Am. **82**, 306–310 (1987).

[14] R. Stoughton, "Measurements of small caliber ballistic shock waves in air," J. Acoust. Soc. Am. **102**, 781–787 (1997).

[15] J. A. Vernon, K. L. Gee, and J. H. Macedone, "Acoustical characterization of exploding hydrogen-oxygen balloons," J. Acoust. Soc. Am. **131**, EL243–EL249 (2012).

[16] K. L. Gee, J. H. Giraud, J. D. Blotter, and S. D. Sommerfeldt, "Near-field acoustic intensity measurements of a small solid rocket motor," J. Acoust. Soc. Am. **128**, EL69–EL74 (2010).

[17] K. L. Gee, J. A. Vernon, and J. H. Macedone, "Auditory risk of exploding hydrogen–oxygen balloons," J. Chem. Ed. **87**, 1039–1044 (2010).

[18] G. Ben-Dor, Shock Wave Reflection Phenomena, 2nd ed. (Springer, Berlin, 2007), pp. 1–38, 247–306.

[19] T. B. Gabrielson, T. M. Marston, and A. A. Atchley, "Nonlinear propagation modeling: Guidelines for supporting measurements," Proc. Noise-Con **114**, 275–285 (2005).

[20] D. K. Wilson, "The sound-speed gradient and refraction in the near ground atmosphere," J. Acoust. Soc. Am. **113**, 750–757 (2003).

[21] D. J. Maglieri and K. J. Plotkin, "Sonic Boom," in Noise Sources, Vol. 1 of Aeroacoustics of Flight Vehicles: Theory and Practice, edited by H. H. Hubbard (Acoustical Society of America, Woodbury, NY, 1995), Chap. 10, pp. 523–525.

[22] F. M. Pestorius and S. B. Williams, "Upper limit on the use of weak-shock theory," J. Acoust. Soc. Am. **55**, 1334–1335 (1974).

Appendix A

Generic_waveform_viewerKEVINEDIT.m
(used to transform the binary acoustic data into pressure vs time waveforms)

```
clear all;
close all;
clc;

PlotSetup %a function listed below
%for kirchoff change "Z" to "R"
pathname='Z:\Faculty\Dr. Gee\Data\2014 Bonneville Boom\Half Mile\';
testname='salt_ID';  % Root test name from Data Recorder
ID=[30];% Test Number
CH=[0 1 2];
SIZE=[22];
fs=50000; % Sampling Frequency (Hz)
N2 = 12;    % 2^N2 is the bin width for the PSD estimate
format long
for k=1:length(ID)
            %go through tests

        for n =1:length(CH) %go through channels
                filename=[pathname,testname,sprintf('%03.0f',ID(k)),'_',...
                   sprintf('%03.0f',CH(n)),'.bin'];

                fid=fopen(filename,'r');
                x=fread(fid,inf,'single');
                fclose(fid);
                dt=1/fs;
                t=0:dt:dt*(length(x)-1);
                if CH(n)==2
                   x=-x;
                end
                % Plot time data
                %subplot(2,1,1)
                hold on
                plot(t,x)
                title(['ID' num2str(ID(k)) ' ' 'Channel' ' ' num2str(CH(n)),' ',num2str(SIZE(k)),'inch'])
                xlabel('Time (s)')
                ylabel('Pressure (Pa)');
                grid on
                % subplot(2,1,2)
                % db=20*log10(x/(20*10^-6));
                % plot(t,db)
                % xlabel('Time (s)')
                % ylabel('dB (re 20 micro Pa)')
                %PowerSpectralDensity(x,fs,N2,1);
        end
end
```

Function: PlotSetup.m
(as used in the script shown above)

```
function PlotSetup(R_L,LineLW,AxesLW,FontS)
% function PlotSetup(R_L,LineLW,AxesLW,FontS)
%
%   R_L    - Right or left monitor (because I use a two-screen system
%   LineLW - LineLineWidth
%   AxesLW - AxesLineWidth
%   FontS  - AxesFontSize
%
% This function sets up the default plotting system to be more conducive
% to presentation and publication.

if nargin < 4; FontS = 20; end
if nargin < 3; FontS = 20; AxesLW = 2; end
if nargin < 2; FontS = 20; AxesLW = 2; LineLW = 2; end
if nargin < 1; R_L = 'l'; end

if strcmp(R_L,'R'); R_L = 'r'; end
if strcmp(R_L,'L'); R_L = 'l'; end

if strcmp(R_L,'r')
set(0,'DefaultFigurePosition',[1390 50 1150 800]);
end
if strcmp(R_L,'l')
set(0,'DefaultFigurePosition',[20 50 1150 800]);
end

set(0,'DefaultAxesLineWidth',AxesLW);
set(0,'DefaultLineLineWidth',LineLW);
set(0,'DefaultAxesFontSize',FontS);
set(0,'DefaultAxesFontName','Times New Roman');
set(0,'DefaultAxesYGrid','on');
set(0,'DefaultAxesXGrid','on');

colvect=[...
   45/255,73/255,121/255;...      blue
   0/255,127.5/255,0/255;...      green
   204/255,34/255,6/255;...       red
   117/255,51/255,183/255;...     purple
   190/255,153/255,32/255;...     yellow
   53/255,142/255,132/255;...     aqua
   240/255,78/255,0/255;...       orange
   198/255,9/255,151/255;...      pink
   ];  % K&M-set

set(0,'DefaultAxesColorOrder',colvect);

set(0,'DefaultAxesLineStyleOrder','-|--')
```